Electronic and transport properties of V-shaped defect zigzag MoS_2 nanoribbons*

Li Xin-Mei(李新梅)[a], Long Meng-Qiu(龙孟秋)[a)†], Cui Li-Ling(崔丽玲)[a)b)], Xiao Jin(肖 金)[a)], and Xu Hui(徐 慧)[a)‡]

[a)] *Institute of Super-microstructure and Ultrafast Process in Advanced Materials, School of Physics and Electronics, Central South University, Changsha* 410083, *China*

[b)] *School of Science, Hunan University of Technology, Zhuzhou* 412007, *China*

(Received 9 August 2013; revised manuscript received 10 September 2013; published online 20 February 2014)

Based on the nonequilibrium Green's function (NEGF) in combination with density functional theory (DFT) calculations, we study the electronic structures and transport properties of zigzag MoS_2 nanoribbons (ZMNRs) with V-shaped vacancy defects on the edge. The vacancy formation energy results show that the zigzag vacancy is easier to create on the edge of ZMNR than the armchair vacancy. Both of the defects can make the electronic band structures of ZMNRs change from metal to semiconductor. The calculations of electronic transport properties depict that the currents drop off clearly and rectification ratios increase in the defected systems. These effects would open up possibilities for their applications in novel nanoelectronic devices.

Keywords: transport property, zigzag MoS_2 nanoribbons, V-shaped defect, first-principles

PACS: 73.63.–b, 73.23.–b **DOI:** 10.1088/1674-1056/23/4/047307

1. Introduction

Molybdenum disulfide (MoS_2) is a kind of typical layered structure semiconductor with an indirect band gap of about 1.3 eV.[1] It is a promising material with highly potential applications in solar cells,[2] photocatalysts,[3,4] solid lubrication,[5,6] etc. It is easy to obtain nanosheet MoS_2 because of the weak van der Waals interaction between the layers of MoS_2 crystal. In recent years, two-dimensional (2D) single-layer MoS_2 sheets have been produced experimentally by chemical exfoliation,[7,8] chemical vapor deposition,[9] epitaxial growth,[10,11] etc. The electronic structures of MoS_2 have also been discussed through calculation. Both experimental and calculation results show that the single-layer MoS_2 is semiconductor with a direct band gap of about 1.8 eV.[1,12] This excellent performance makes it a very interesting substitute/complement to graphene in semiconducting applications such as transistors,[13,14] small-signal amplifiers,[15] and ultraviolet photodetectors.[16] Recently, with the development of experimental technique, quasi one-dimensional MoS_2 nanoribbons (MNRs) have been successfully synthesized.[17,18] Theoretical studies showed that the nanoribbons exhibit unusual physical properties: irrespective of the width of ribbons, zigzag MoS_2 nanoribbons are ferromagnetic and metallic, while armchair MoS_2 nanoribbons (AMNRs) are non-magnetic and semiconducting.[19–21] By further investigation, Pan and Zhang[22] found that when strain is exerted along the axis, the band gaps of AMNRs decrease with the increasing of strain, and their direct band gaps subjected to the weak strain change into indirect ones with the strain increasing up to 10%.

Because the electronic structures and transport properties of graphene nanoribbons (GNRs) can be modulated by edge modification,[23–26] as a kind of graphene-like nanomaterial, research on the edge modification on MNRs has aroused a great deal of interest. Yang *et al.*[27] reported that when Mg atoms are absorbed on the double-side of ZMNR, a maximum theoretical capacity of 223.2 mAh·g^{-1} can be achieved. Erdogan *et al.*[28] found that the edge passivation influences the electronic and transport properties of MNRs, especially for zigzag-edged nanoribbons. Meanwhile, Pan and Zhang[21] showed that the stabilities and electronic properties of MNRs strongly depend on their chiralities and edge structures. In addition, the metallic ZMNRs can be changed into semiconductors or half-metals by controlling the dangling states on the edges with hydrogen. It is also found that a S vacancy on the edge of the ribbon can change the electronic structures of MNRs.[29] Furthermore, we have found that the V-shaped notches on the edge can modulate the transport properties of GNRs effectively.[30] Nevertheless, to the best of our knowledge, effects of vacancy defects on the edge on transport properties of ZMNRs have been scarcely investigated.

In this work, we study the electronic structures and electronic transport properties of ZMNRs with armchair and zigzag V-shaped vacancy defects on one edge, and perfect on the other. The model structures are shown in Figs. 1(a)–1(d),

*Project supported by the National Natural Science Foundation of China (Grant Nos. 21103232, 51272291, and 11174371).

†Corresponding author. E-mail: mqlong@csu.edu.cn

‡Corresponding author. E-mail: cmpxhg@csu.edu.cn

© 2014 Chinese Physical Society and IOP Publishing Ltd

where the perfect ZMNR, ZMNR with armchair V-shaped vacancy, and zigzag V-shaped vacancy on the edge are labeled as 4-Z, 4-AZ, and 4-ZZ, respectively. Here, 4 denotes the number of Mo–S_2 bases in the unit cell of perfect nanoribbon. For each system, the z direction is parallel to the transport direction. In the calculations of electronic transport properties, we use two-probe systems, which contain three regions (Fig. 1): left electrode, right electrode, and central region. The electrodes are two semi-infinite perfect ZMNRs.

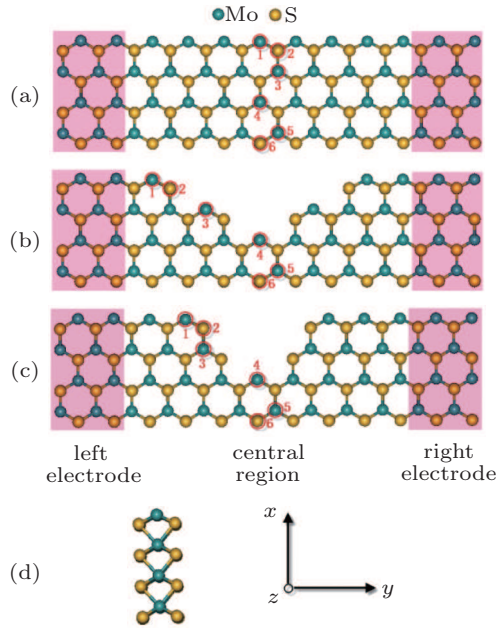


Fig. 1. (color online) Two-probe systems: (a) 4-Z, (b) 4-AZ, (c) 4-ZZ, (d) side view of the systems.

2. Computational details

The geometrical optimizations and electronic structure results of the MNRs are based on first-principles plane wave calculations within density functional theory (DFT)[31,32] and the Perdew–Wang 91 (PW91) exchange-correlation functional under the spin-unpolarized generalized gradient approximation (GGA),[33] as implemented in the Vienna *ab initio* simulation package (VASP)[34,35] with a projector augmented wave (PAW) scheme. The vacuum layer thickness (defined in Fig. 1) is set to be 15 Å to avoid the artificial Coulomb interactions between the contents in two neighboring cells. In our calculations, a plane wave cutoff energy of 400 eV, a Monkhorst–Pack k-point sampling of $1\times1\times21$ with a convergence criterion of 10^{-5} eV and the maximum Hellmanm–Feynman forces acting on each atom less than 0.05 eV/Å upon ionic relaxation are chosen to achieve the balance between calculation efficiency and accuracy.

The electronic transport properties are calculated by using the Atomistix Toolkit (ATK) package,[36–38] which is based on real-space, NEGF formalism, and the DFT. In calculations, the parameters are set as follows: k-point grid is $1\times1\times500$, mesh cutoff of all atoms is 150 Ry, all the configurations are relaxed until their force tolerance is less than 0.05 eV/Å. The current through the molecular junction as a function of the applied external bias can be obtained by using the Landauer–Büttiker formula,[39]

$$I(V) = \frac{2e}{h}\int [f(E-\mu_{\rm L}) - f(E-\mu_{\rm R})]T(E,V)\,{\rm d}E, \quad (1)$$

where e, h, and f are the electron charge, Planck's constant, and Fermi function, respectively, E is the energy, $\mu_{\rm L/R}$ is the electrochemical potential of the left/right electrode, and the difference in electrochemical potential is given by $\mu_{\rm L} = \mu(0) - eV/2$ and $\mu_{\rm R} = \mu(0) + eV/2$ with V being the applied voltage, $T(E,V)$ is the quantum mechanical transmission probability of electrons, and it can be given as

$$T(E,V) = {\rm tr}[\Gamma_{\rm L}(E,V)G^{\rm R}(E,V)\Gamma_{\rm R}(E,V)G^{\rm A}(E,V)]. \quad (2)$$

Here, $\Gamma_{\rm L/R}$ is the contact broadening functions associated with the left/right electrode and $G^{\rm R/A}$ is the retarded/advanced Green's function of the central region.

3. Results and discussion

The stability analysis for a system is very important since it can determine whether this structure can be realized experimentally. Thus, firstly, we calculate the vacancy formation energies to estimate the stability of the defected system. Here the vacancy formation energy $E_{\rm f}^{\rm vac}$ is defined as[40–42]

$$E_{\rm f}^{\rm vac} = (E_{\rm defect} + m.E_{\rm Mo} + n.E_{\rm S}) - E_{\rm perfect}, \quad (3)$$

where $E_{\rm defect}$ and $E_{\rm perfect}$ are the total energies of ZMNRs with and without V-shaped vacancy defects on the edge, $E_{\rm Mo}$ and $E_{\rm S}$ are the energies of individual free Mo and S atoms, and m or n is the number of Mo or S atoms removed from the perfect system. Since the configurations of 4-Z, 4-AZ, and 4-ZZ are $Mo_{32}S_{64}$, $Mo_{25}S_{54}$, and $Mo_{27}S_{58}$, respectively, the values of (m,n) are (7, 10) for 4-AZ and (5, 6) for 4-ZZ. Generally, those with lower vacancy formation energies are more stable, and then easier to form. The calculated vacancy formation energies are 92.74 eV and 61.98 eV for 4-AZ and 4-ZZ, respectively. Thus, we can predict that the zigzag V-shaped vacancy on the edge of ZMNR will be created more easily than the armchair one.

We compare the band structures of the perfect 4ZMNR folded according to the Brillouin zone of an MoS_2 cell, with those of the V-shaped defect $Mo_{25}S_{54}$ and $Mo_{27}S_{58}$ cells as shown in Fig. 2. We can see that the perfect ZMNR has metallic properties. However, due to the Fermi levels (FLs) positioned at the valance bands, both of the defected systems become p-type semiconductors with the band gaps about 0.15 eV (4-AZ) and 0.1 eV (4-ZZ), respectively, as illustrated in Figs. 2(b) and 2(c). One or two flat bands have been introduced near the FLs in the band structures of 4-AZ and 4-ZZ, suggesting the localization of these states. We present the band structures for 5-Z, 6-Z and their corresponding defected systems in Fig. 3. Here, the sizes of defects in 5-AZ and 6-AZ are

the same as in 4-AZ, and those in 5-ZZ and 6-ZZ are the same as in 4-ZZ. From Fig. 3, we can also find that there are metallic characteristics for perfect ZMNRs, but p-type semiconductor characteristics for the systems with V-shaped vacancy defects on the edge.

To understand the band structures shown in Fig. 2 further, we put forward the total density of state (TDOS) and partial density of state (PDOS) each as a function of energy as presented in Fig. 4. We can find clearly that there is no band gap near the FL for 4-Z system, indicating the metallic characteristic. But in each defected system, there is a narrow gap above the FL, meaning the p-type semiconductor characteristic. So, we consider that in the defected systems $Mo_{25}S_{54}$ and $Mo_{27}S_{58}$, the number of S atoms is more than twice that of Mo atoms because of the edge vacancy defects, and then the redundant S atoms might provide more holes for transporting. Moreover, the PDOS curves (Fig. 4(a)) of 4-Z show that the contributions to the TDOS mainly come from the 4d-orbits and 3p-orbits of edge atoms (1-Mo and 6-S). But for the defected systems (Figs. 4(b) and 4(c)), the contributions of 4d-orbits of Mo atoms on the edge of V-shaped vacancy (3-Mo and 4-Mo) to the TDOS are much more than for the perfect system, especially to the DOS peaks very close to the FLs. Maybe, which is the reason why the localized states occur near the FLs.

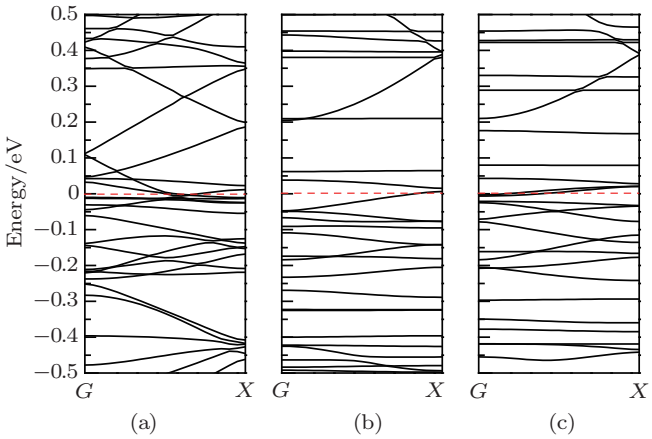


Fig. 2. (color online) The calculated band structures of (a) 4-Z, (b) 4-AZ, and (c) 4-ZZ, respectively. The zero of energy is set at Fermi level (red dotted line) in each system.

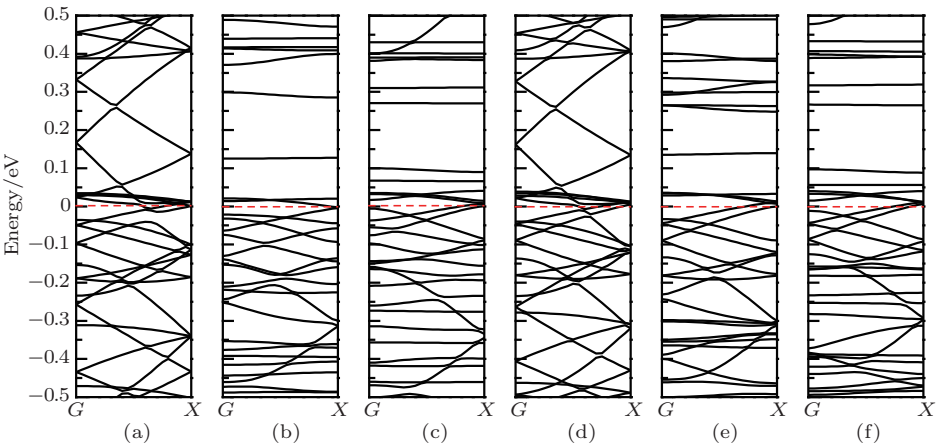


Fig. 3. (color online) Calculated band structures of (a) 5-Z, (b) 5-AZ, (c) 5-ZZ, (d) 6-Z, (e) 6-AZ, and (f) 6-ZZ, respectively. The zero of energy is set at Fermi level (red dotted line) in each system.

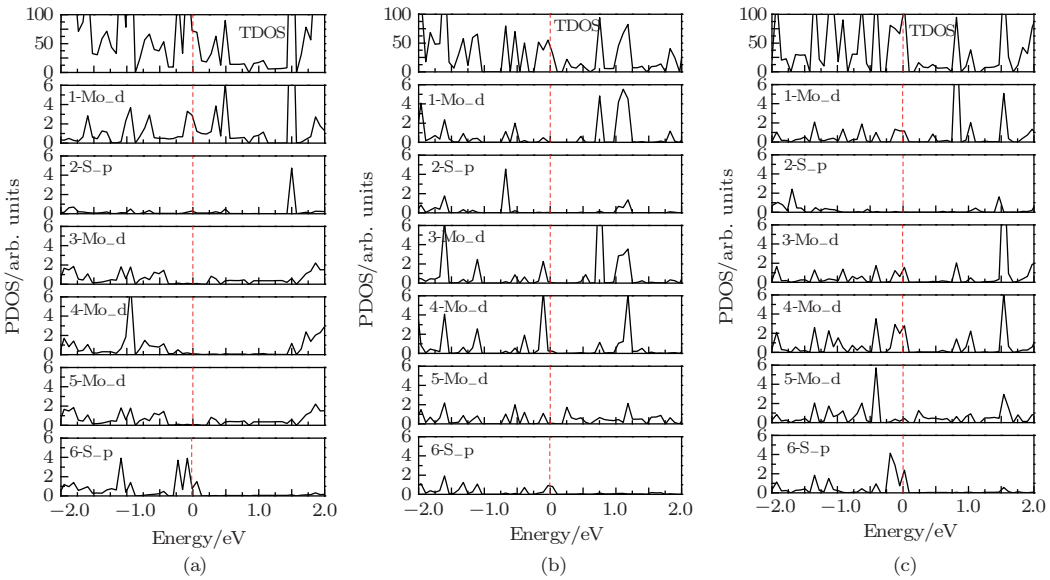


Fig. 4. (color online) TDOS and PDOS of (a) 4-Z, (b) 4-AZ, and (c) 4-ZZ, respectively. The zero of energy is set at Fermi level (red dotted line) in each system.

In order to investigate the effect of V-shaped vacancy defects on the electronic transport properties of ZMNRs, we carry out first-principles calculations of current–voltage (I–V) curves by using two-probe systems (shown in Fig. 1). Figure 5(a) shows the I–V curves in a bias range of [−2.0 V, 2.0 V] for systems 4-Z, 4-AZ, and 4-ZZ. It can be clearly seen that the current increases rapidly in 4-Z at a very low bias, confirming the metallic characteristic of the system, but a wide zero-current flat around the zero bias is present in the I–V curve of 4-AZ or 4-ZZ, indicating the semiconductor characteristic. And their current intensities is in the order of $I_{4-Z} > I_{4-AZ} > I_{4-ZZ}$ under the same bias voltage, which means that in a lower bias range, the V-shaped vacancy defects on the edge will suppress the charge transport of ZMNRs. More interestingly, figure 5(a) shows that the I–V curves are asymmetric for all the systems. Usually, this asymmetry property implies a rectification effect of the system.[43,44] So we present the rectification ratios of all systems as shown in the inset of Fig. 5(a). The rectification ratio is defined as

$$R(V) = \left|\frac{I(+V)}{I(-V)}\right|. \tag{4}$$

Here, $R(V) = 1$ indicates no rectification, and $R(V) > 1$ means the current in the positive direction is higher than that in the negative direction. From the rectification ratio curves, we can find that the rectification ration values of 4-AZ and 4-ZZ are larger than that of 4-Z, which results from the greater asymmetry in the V-shaped vacancy-defected ZMNRs than in the perfect one.

As is well known, when the external bias is very low, the conductance characteristic can be understood from the transmission spectrum $T(E,V)$ of the system at zero bias ($V = 0$). As shown in Fig. 5(b), we can see that the transmission spectrum for 4-Z is much stronger than those for 4-AZ and 4-ZZ, causing the current intensity of 4-Z to be largest in the current intensities of the three systems. There are transmission gaps (TGs) only in 4-AZ and 4-ZZ. So system 4-Z displays the metallic characteristic and systems 4-AZ and 4-ZZ exhibit semiconductor characteristics.

Usually, the local density of states (LDOS) can give an essential explanation for the electronic transport properties of a system. Then, in Fig. 6, we show the LDOSs at FLs at zero bias voltage for the three systems above. It is shown clearly that the edge states play an important role in determining the electronic transport properties for all of the calculated systems, which is consistent very well with the conclusions reported earlier.[19–21] Meanwhile, we can find that for the perfect system 4-Z (Fig. 6(a)), the LDOSs are almost assigned over the edges of the whole ribbon, and thus its larger transmission spectrum and larger current can be obtained. But for systems 4-AZ (Fig. 6(b)) and 4-ZZ (Fig. 6(c)), due to the introducing of V-shaped vacancy defects on the edge of ZMNR, the localized edge electronic states occur. So, their transport properties, especially those of system 4-ZZ (Fig. 5), have been suppressed strongly.

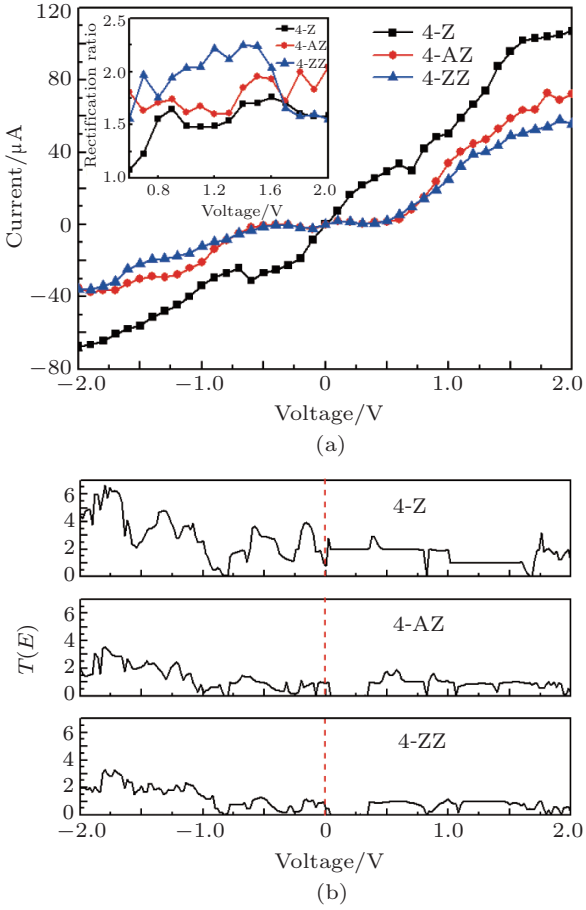


Fig. 5. (color online) (a) I–V curves of 4-Z, 4-AZ, and 4-ZZ; (b) transmission spectra for 4-Z, 4-AZ, and 4-ZZ systems at zero bias voltage. The zero of energy is set at Fermi level (red dotted line) in each system. The inset shows the rectification ratios of the three systems.

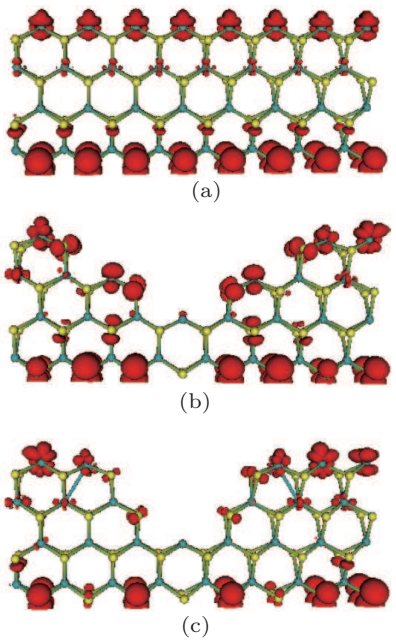


Fig. 6. (color online) The LDOSs at 0 eV for systems (a) 4-Z, (b) 4-AZ, and (c) 4-ZZ, respectively.

4. Conclusions

We perform the first-principles investigations of electronic structures and transport properties of V-shaped defect ZMNRs. The calculations of vacancy formation energies reveal that the zigzag vacancy is easier to create on the edge of ZMNRs than the armchair one. Unlike the metallic characteristic of perfect ZMNR, the vacancy-defected system presents p-type semiconductor behavior. The current is reduced remarkably when introducing a V-shaped defect on the edge of ZMNRs. And because of the greater asymmetry in the defected system, the asymmetric I–V properties and rectification effect become more obvious. Moreover, the electronic structures and transport properties depend on the defect type. All these characteristics might be potentially useful in fabricating ZMNR-based devices.

References

[1] Tawinan C and Walter R L L 2012 *Phys. Rev. B* **85** 205302
[2] Fornarini L, Stirpe F and Scrosati B 1981 *Solar Energy Mater.* **5** 107
[3] Zong X, Yan H J, Wu G P, Ma G J, Wen F Y, Wang L and Li C 2008 *J. Am. Chem. Soc.* **130** 7176
[4] Xiang Q J, Yu J G and Jaroniec 2012 *J. Am. Chem. Soc.* **134** 6575
[5] Hu K H, Hu X G, Wang J, Xu Y F and Han C L 2012 *Tribol. Lett.* **47** 79
[6] Tian L, Zhou Q L, Zhao K, Shi Y L, Zhao D M, Zhao S Q, Zhao H, Bao R M, Zhu S M, Miao Q and Zhang C L 2011 *Chin. Phys. B* **20** 010703
[7] Eda G, Yamaguchi H, Voiry D, Fujita T, Chen M W and Chhowalla M 2011 *Nano Lett.* **11** 5111
[8] Coleman J N, Lotya M, O'Neill A, Bergin S D, King P J, Khan U, Young K, Gaucher A, De S, Smith R J, Shvets I V, Arora S K, Stanton G, Kim H Y, Lee K, Kim G T, Duesberg G S, Hallam T, Boland J J, Wang J J, Donegan J F, Grunlan J C, Moriarty G, Shmeliov A, Nicholls R J, Perkins J M, Grieveson E M, Theuwissen K, McComb D W, Nellist P D and Nicolosi V 2011 *Science* **331** 568
[9] Lee Y H, Zhang X Q, Zhang W J, Chang M T, Lin C T, Chang K D, Yu Y C, Qang J T W, Chang C S, Li L J and Lin T W 2012 *Adv. Mater.* **24** 2320
[10] Smith R J, King P J, Lotya M, Wirtz C, Khan U, De S, O'Neill A, Duesberg G S, Grunlan J C, Moriarty G, Chen J, Wang J Z, Minett A I, Nicolosi V and Coleman J N 2011 *Adv. Mater.* **23** 3944
[11] Shi Y M, Zhou W, Lu A Y, Fang W J, Lee Y H, Hsu A L, Kim S M, Kin K K, Yang H Y, Li L J, Idrobo J C and Kong J 2012 *Nano Lett.* **12** 2784
[12] Lee H S, Min S W, Chang Y G, Park M K, Nam T, Kim H, Kim J H, Ryu S and Im S 2012 *Nano Lett.* **12** 3695
[13] Zhang Y J, Ye J T, Matsuhashi Y and Iwasa Y 2012 *Nano Lett.* **12** 1136
[14] Yin Z Y, Li H, Li H, Jiang L, Shi Y M, Sun Y H, Lu G, Zhang Q, Chen X D and Zhang H 2012 *ACS Nano.* **6** 74
[15] Radisavljevic B, Whitwick M B and Kis A 2012 *Appl. Phys. Lett.* **101** 043103
[16] Alkis S, Öztas T, Aygün L E, Bozkurt F, Okyay A K and Ortac B 2012 *Opt. Express* **20** 21815
[17] Li Q, Newberg J T, Walter E C, Hemminge R J C and Penner R M 2004 *Nano Lett.* **4** 277
[18] Wang Z, Li H, Liu Z, Shi Z, Lu J, Suenaga K, Joung S K, Okazaki T, Gu Z, Zhou J, Gao Z, Li G, Sanvito S, Wang E and Lijima S 2010 *J. Am. Chem. Soc.* **132** 13840
[19] Li Y F, Zhou Z, Zhang S B and Chen Z F 2008 *J. Am. Chem. Soc.* **130** 16739
[20] Ataca C, Sahin H, Aktürk E and Ciraci S 2011 *J. Phys. Chem. C* **115** 3934
[21] Pan H and Zhang Y W 2012 *J. Mater. Chem.* **22** 7280
[22] Pan H and Zhang Y W 2012 *J. Phys. Chem. C* **116** 11752
[23] Cuong N T, Otani M and Okada S 2013 *Phys. Rev. B* **87** 045424
[24] Yu X X, Xie Y E, Ouyang T and Chen Y P 2012 *Chin. Phys. B* **21** 107202
[25] Chen L N, Ma S S, Ouyang F P, Wu X Z, Xiao J and Xu H 2010 *Chin. Phys. B* **19** 097301
[26] Tian H Y and W J 2012 *Chin. Phys. B* **21** 017203
[27] Yang S Q, Li D X, Zhang T R, Tao Z L and Chen J 2012 *J. Phys. Chem. C* **116** 1307
[28] Erdogan E, Popov I H, Enyashin A N and Seifert G 2012 *Eur. Phys. J. B* **85** 33
[29] Shidpour R and Manteghian M 2010 *Nanoscale* **2** 1429
[30] Zhang X J, Chen K Q, Tang L M and Long M Q 2011 *Phys. Lett. A* **375** 3319
[31] Kohn W and Sham L J 1965 *Phys. Rev. A* **140** 1133
[32] Hohenberg P and Kohn W 1964 *Phys. Rev. B* **136** 864
[33] John P P, Kieron B and Matthias E 1996 *Phys. Rev. Lett.* **77** 3865
[34] Kresse G and Hafner J 1993 *Phys. Rev. B* **47** 558
[35] Kresse G and Furthmuller J 1996 *Phys. Rev. B* **54** 11169
[36] Brandbyge M, Mozos J L, Ordejón P, Taylor J and Stokbro K 2002 *Phys. Rev. B* **65** 165401
[37] Zeng M G, Feng Y P and Liang G C 2011 *Nano Lett.* **11** 1369
[38] See http://quantumwise.com/, for ATOMISTIX TOOLKIT
[39] Buttiker M, Imry Y, Landauer R and Pinhas S 1985 *Phys. Rev. B* **31** 6207
[40] Dan X, Yao K L, Gao G Y and Ma G Q 2013 *Chin. Phys. B* **22** 047507
[41] Qiao Z J, Chen G D, Ye H G, Wu Y L, Niu H B and Zhu Y Z 2012 *Chin. Phys. B* **21** 087101
[42] Pan H, Feng Y P, Wu Q Y and Huang Z G 2008 *Phys. Rev. B* **77** 125211
[43] Xu H J and Li X J 2008 *Appl. Phys. Lett.* **93** 172105
[44] Aparecido-Ferreeira A, Miyazaki H, Li S L, Komatsu K, Nakaharai S and Tsukaqoshi K 2012 *Nanoscale* **4** 7842